# Gait Generation of 6-DOF Biped Robot on Inclined Deformable Terrain Using Nonlinear Inverted Pendulum

Sunil Gora
Indian Institute of Technology, Kanpur
Uttar Pradesh, INDIA
sunilg@iitk.ac.in

Shakti S. Gupta
Indian Institute of Technology, Kanpur
Uttar Pradesh, INDIA
ssgupta@iitk.ac.in

Ashish Dutta
Indian Institute of Technology, Kanpur
Uttar Pradesh, INDIA
adutta@iitk.ac.in

## ABSTRACT

In this paper, a 6-DOF biped's gait is generated based on the motion of the center of mass and the contact point of a nonlinear inverted pendulum (NIP). For walking on deformable terrain, the foot-terrain interaction is modeled using terrain stiffness and damping. The impact dynamics of the NIP model is used to obtain the curve of capture to stop the motion and the curve of equal local energy for walking with equal minimum velocity. The step length obtained from the intersection of the energy curve of the NIP and the terrain is used for the swing leg ankle trajectory. The center of mass and contact point trajectories of the NIP are used in the trajectory generation of the hip-link and the stance leg's ankle, and the joint angles of the biped are obtained from the inverse kinematics. The floating-base dynamics is used to compare the actual and desired center of mass trajectories of the biped robot. The energy analysis of the biped validates the footstep planning on deformable terrain. The joint torques of the actuated joints are obtained from the inverse dynamics, and the actuation energy is shown to be negligible for energy-efficient walking. The dynamic stability of the biped's gait is also analyzed based on the rotation of the foot on the deformable terrain.

## CCS CONCEPTS

• **Computer systems organization → Robotics**; *Robotic autonomy*; Robotic components.

## KEYWORDS

biped robot, gait generation, nonlinear inverted pendulum, deformable terrain

**ACM Reference Format:**
Sunil Gora, Shakti S. Gupta, and Ashish Dutta. 2023. Gait Generation of 6-DOF Biped Robot on Inclined Deformable Terrain Using Nonlinear Inverted Pendulum. In *Advances In Robotics - 6th International Conference of The Robotics Society (AIR 2023), July 5–8, 2023, Ropar, India.* ACM, New York, NY, USA, 6 pages. https://doi.org/10.1145/3610419.3610445


*AIR 2023, July 5–8, 2023, Ropar, India*

ACM ISBN 978-1-4503-9980-7/23/07…$15.00
https://doi.org/10.1145/3610419.3610445

## 1 INTRODUCTION

Energy-efficient locomotion of the legged robots on different terrains requires a combination of active and passive walking. In active walking, actuation energy is utilized to control the robot's motion for walking with dynamic stability constraint of zero moment point (ZMP) [17]. For a dynamically stable walking trajectory, the actuated joints are controlled to ensure that the position of the ZMP is inside the support polygon. The active dynamic walking of biped on inclined terrain [14, 19], stairs [15] and 3D terrain [8] has been achieved using the ZMP criterion. For 3D walking pattern generation, Kajita et. al. [6] used a linear inverted pendulum model (LIPM) to simplify the dynamics of biped by constraining the motion of the center of mass along an arbitrarily defined plane. In [12], the orbital energy of LIPM is used to determine the foot placement position called the capture point to stop the motion of the robot. State-dependent footstep planning is also explored to avoid dynamic obstacles on flat terrain in [1]. For stable biped locomotion on uneven terrain, Kuindersma et al. [7] used a footstep planner with optimization algorithms based on the complexity of motion and kinematic constraints.

In passive walking, gravity generates the driving force, and the loss of kinetic energy is compensated by the change in potential energy [10]. The mechanical design of a passive walker employing the control of active walking is utilized in 3D passive dynamic walking on flat terrain in [16]. The footstep planning of a passive walker can generate an energy-efficient biped gait for walking on uneven terrain. Crews et al. [3] presented the energy regions of the nonlinear inverted pendulum (NIP) for walking on an uneven terrain.

The dynamic stability criterion based on rigid contact is not sufficient for locomotion of bipedal robots on deformable terrains like grass, sand and rocks. Xiong et al. [18] used an effective support area on deformable granular terrain to study the stability of an inverted pendulum. Mesesan et al. [11] studied the stabilization of the stance foot on compliant terrain using a damping wrench with reference trajectory generated by the divergent component of motion. In [4], the floating-base dynamics of biped is used with the ground deformation in contact dynamics. For biped walking on a deformable terrain, the movement of the center of pressure will rotate the foot about the ankle. This will reduce the projection of the foot area on the plane perpendicular to the direction of gravity. Also, the deformation of the terrain will affect the motion of the center of mass which the NIP model can incorporate using contact modeling. The NIP model with foot-terrain interaction forces is used for footstep planning of biped on deformable terrain in [5], however, the footstep planning is not validated for dynamically stable walking. The biped gait generation on inclined deformable terrain with footstep planning is not reported in the literature to the best of authors' knowledge. The 6-DOF biped robot walking on deformable terrain with footstep planning using the NIP model is presented in this paper. The step length of biped is determined based on footstep planning using the energy curves of the model. The 6-DOF biped gait generation from the trajectory of the center of mass and contact point of NIP is illustrated in this paper.

The rest of the paper is organized as follows: The dynamics of the 6-DOF biped robot and NIP model are discussed in Section. 2. In Section 3, the expressions of the curve of capture and the curve of equal local energy are derived. Section 4 presents the simulation results of the 6-DOF biped robot walking on hard and deformable terrain. The conclusions and future scope of work are discussed in Section 5.

## 2 DYNAMIC MODELING OF BIPED ROBOT

The 6-DOF model of a biped robot and the simplified NIP model are shown in Fig. 1. The governing equations of the 6-DOF biped are obtained in terms of mass ($m$), mass moment of inertia about $y$-axis $I_{yy}$, and the positions and velocities of the center of mass and the center of the stance leg foot. The motion of the NIP model is generated on the deformable terrain. The trajectories of the center of mass and the contact point with step length are used for biped gait generation as shown in Fig. 1.

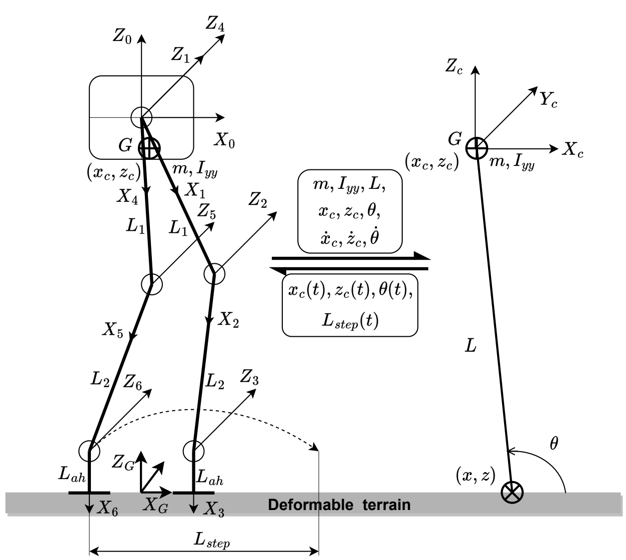


**Figure 1: 6-DOF biped robot and simplified nonlinear inverted pendulum model**

For the 6-DOF biped model, the floating-base representation is used with the base frame attached to the center of the hip-link. The transformation of the base frame with respect to the ground frame is obtained using virtual joints. The Denavit–Hartenberg (DH) parameters of the 6-DOF biped robot are given in Table. 1.

**Table 1: DH parameters of 6-DOF biped robot with floating-base**

| Parent (j) | Child (i) | $\theta_i$ | $d_i$ | $a_j$ | $\alpha_j$ |
|---|---|---|---|---|---|
| G | b1 | $90^o$ | $z_0$ | 0 | $0^o$ |
| b1 | b2 | $0^o$ | $x_0$ | 0 | $90^o$ |
| b2 | b3 | $\theta_{y0}$ | 0 | 0 | $90^o$ |
| b3 | 0 | $0^o$ | 0 | 0 | $90^o$ |
| 0 | 1 | $\theta_1$ | 0 | 0 | $-90^o$ |
| 1 | 2 | $\theta_2$ | 0 | $L_1$ | $0^o$ |
| 2 | 3 | $\theta_3$ | 0 | $L_2$ | $0^o$ |
| 0 | 4 | $\theta_4$ | 0 | 0 | $-90^o$ |
| 4 | 5 | $\theta_5$ | 0 | $L_1$ | $0^o$ |
| 5 | 6 | $\theta_6$ | 0 | $L_2$ | $0^o$ |

The generalized joint coordinates of the biped in terms of virtual joint coordinates and actuated joint coordinates are written as

$$\boldsymbol{q} = \begin{bmatrix} \boldsymbol{q}_0 \\ \boldsymbol{q}_\theta \end{bmatrix}, \tag{1}$$

where, $\boldsymbol{q}_0 \in \boldsymbol{R}^{3\times1}$ is the vector of unactuated virtual joints of the base frame on the hip-link and $\boldsymbol{q}_\theta \in \boldsymbol{R}^{6\times1}$ is the vector of actuated joints of the robot, which can be written as

$$\boldsymbol{q}_0 = \begin{bmatrix} z_0 & x_0 & \theta_{y0} \end{bmatrix}^T, \tag{2}$$

$$\boldsymbol{q}_\theta = \begin{bmatrix} \theta_1 & \theta_2 & \theta_3 & \theta_4 & \theta_5 & \theta_6 \end{bmatrix}^T. \tag{3}$$

The joint angles are obtained from the trajectories of the center of the hip-link and ankles of the stance and swing legs from inverse position kinematics [4]. The MATLAB inbuilt function 'spline' is used for the cubic spline data interpolation of trajectories.

### 2.1 Inverse dynamics of 6-DOF biped robot

The equations of motion of the 6-DOF biped robot are written as

$$\begin{bmatrix} \boldsymbol{I}_0 & \boldsymbol{I}_{0\theta} \\ \boldsymbol{I}_{0\theta}^T & \boldsymbol{I}_\theta \end{bmatrix} \begin{bmatrix} \ddot{\boldsymbol{q}}_0 \\ \ddot{\boldsymbol{q}}_\theta \end{bmatrix} + \begin{bmatrix} \boldsymbol{c}_0 \\ \boldsymbol{c}_\theta \end{bmatrix} = \begin{bmatrix} \boldsymbol{0} \\ \boldsymbol{\tau}_\theta \end{bmatrix} + \begin{bmatrix} \boldsymbol{J}_{c_0}^T \\ \boldsymbol{J}_{c\theta}^T \end{bmatrix} \boldsymbol{w}_c. \tag{4}$$

Here, $\boldsymbol{I}_0 \in \boldsymbol{R}^{3\times3}$ is the inertia matrix of the base, $\boldsymbol{I}_\theta \in \boldsymbol{R}^{6\times6}$ is the inertia matrix of the legs, $\boldsymbol{I}_{0\theta} \in \boldsymbol{R}^{3\times6}$ is the coupling inertia matrix, $\boldsymbol{c}_0 \in \boldsymbol{R}^{3\times1}$ and $\boldsymbol{c}_\theta \in \boldsymbol{R}^{6\times1}$ are the vectors of position and velocity dependent terms associated with the base and legs, respectively, $\boldsymbol{\tau}_\theta \in \boldsymbol{R}^{6\times1}$ is the joint torques vector, $\boldsymbol{J}_{c_0} \in \boldsymbol{R}^{6\times3}$ and $\boldsymbol{J}_{c\theta} \in \boldsymbol{R}^{6\times6}$ are the jacobian matrices of the base and legs, respectively, $\boldsymbol{w}_c \in \boldsymbol{R}^{6\times1}$ is the vector of moments and forces acting at the ankles due to contact forces.

The inverse dynamics solution involves forward dynamics of floating-base, which can be obtained by solving the following equation

$$\boldsymbol{I}_0\ddot{\boldsymbol{q}}_0 + \boldsymbol{I}_{0\theta}\ddot{\boldsymbol{q}}_\theta + \boldsymbol{c}_0 = \boldsymbol{J}_{c_0}^T\boldsymbol{w}_c. \tag{5}$$

Subsequently, the joint torques are obtained from

$$\boldsymbol{\tau}_\theta = \boldsymbol{I}_{0\theta}^T\ddot{\boldsymbol{q}}_0 + \boldsymbol{I}_\theta\ddot{\boldsymbol{q}}_\theta + \boldsymbol{c}_\theta - \boldsymbol{J}_{c\theta}^T\boldsymbol{w}_c. \tag{6}$$

## 2.2 Dynamics of nonlinear inverted pendulum

The nonlinear inverted pendulum (NIP) of mass $m$, mass moment of inertia about $y$-axis, $I_{yy}$ and distance of the center of mass from the contact point $L$ is considered as shown in Fig. 1. The equations of motion of the NIP can be written as

$$\boldsymbol{I}_p \ddot{\boldsymbol{q}}_p + \boldsymbol{c}_p = \boldsymbol{f}_p, \tag{7}$$

where, $\boldsymbol{I}_p \in \boldsymbol{R}^{3\times3}$ is the inertia matrix, $\boldsymbol{q}_p \in \boldsymbol{R}^{3\times1}$ is the vector of joint coordinates, $\boldsymbol{c} \in \boldsymbol{R}^{3\times1}$ is the vector of the centrifugal, coriolis and gravitational forces and $\boldsymbol{f}_p \in \boldsymbol{R}^{3\times1}$ is the vector of the contact forces. The expressions for $\boldsymbol{I}_p$,$\boldsymbol{q}_p$,$\boldsymbol{c}_p$ and $\boldsymbol{f}_p$, respectively, are as follows:

$$\boldsymbol{I}_p = \begin{bmatrix} m & 0 & -mL\sin\theta \\ 0 & m & mL\cos\theta \\ -mL\sin\theta & mL\cos\theta & I_{yy} + mL^2 \end{bmatrix}, \tag{8}$$

$$\boldsymbol{q}_p = \begin{bmatrix} x \\ z \\ \theta \end{bmatrix}, \tag{9}$$

$$\boldsymbol{c}_p = \begin{bmatrix} -mL\dot{\theta}^2\cos\theta \\ mg - mL\dot{\theta}^2\sin\theta \\ mgL\cos\theta \end{bmatrix}, \text{and} \tag{10}$$

$$\boldsymbol{f}_p = \begin{bmatrix} F_x \\ F_z \\ 0 \end{bmatrix}. \tag{11}$$

In Eq. (11), the forces $F_x$ and $F_z$ are determined from the spring-damper contact model [5]. The normal and tangential terrain stiffness are denoted by $k_n$ and $k_t$, respectively, the damping ratio is denoted by $\zeta$, and $\mu$ is the coefficient of friction. The total mechanical energy of the pendulum is given by

$$E = \frac{1}{2}(I_{yy} + mL^2)\dot{\theta}^2 + mg(z + L\sin\theta). \tag{12}$$

# 3 ENERGY CURVES OF NONLINEAR INVERTED PENDULUM

The pre and post-impact configurations denoted by (-) and (+) in the superscript for stance leg transition from the contact point $(x, z)$ to $(x + \Delta x, z + \Delta z)$ are determined using inverse position kinematics [2]. The solution of angles $\theta^-$ and $\theta^+$ is obtained as

$$\theta^+ = \text{atan2}(\Delta z, \Delta x) - \text{atan2}(\sin\alpha, \cos\alpha - 1), \tag{13}$$

$$\theta^- = \theta^+ + \alpha. \tag{14}$$

Here,

$$\alpha = \text{atan2}(\pm\sqrt{4L^2(\Delta x^2 + \Delta z^2) - (\Delta x^4 + \Delta z^4) - 2\Delta x^2\Delta z^2}, \\ 2L^2 - (\Delta x^2 + \Delta z^2)). \tag{15}$$

The conservation of angular momentum about the foot placement point provides the post-impact angular velocity as

$$\dot{\theta}^+ = \dot{\theta}^- \cos\phi, \tag{16}$$

where,

$$\cos\phi = \frac{I_{yy} + mL^2\cos\alpha}{I_{yy} + mL^2}. \tag{17}$$

The energy loss during the change of stance leg includes loss of kinetic energy due to impact and potential energy loss due to ground deformation. The energy loss due to the deformation of the terrain is determined using the stiffness of the terrain $k_n$ and the energy loss due to impact is obtained using Eq. (12) and (16) as

$$E^- - E^+ = mg\left(\frac{mg}{k_n}\right) + \frac{1}{2}(I_{yy} + mL^2)(\dot{\theta}^-)^2\sin^2\phi. \tag{18}$$

The capture point is the foot placement position where the remaining kinetic energy is equivalent to the energy required to gain maximum potential energy, i.e., $E^+ = P_{max}$. Using Eq. (12) and (18), the expression for pre-impact energy is obtained as

$$E^- = mg(z + L\sin\theta^-) + \frac{mg(\Delta z + L(1 - \sin\theta^-))}{\cos^2\phi}. \tag{19}$$

The curve of equal local energy is the locus of foot placement positions on which the loss of kinetic energy equals the loss of potential energy. The pre-impact energy for the curve of equal local energy is obtained from

$$E^- = mg(z + L\sin\theta^-) - \frac{mg\Delta z}{\sin^2\phi}. \tag{20}$$

The energy curves of NIP are obtained by checking the pre-impact energy condition of Eqs. (19) and (20) for $\Delta x$ and $\Delta z$ varied over the reachable workspace. The foot placement position is the intersection point of the energy curve and the inclined terrain. The inclined 2D terrain is represented using a straight-line equation of slope angle $\theta_g$ about Y-axis from the horizontal axis and passing through the initial contact point $(x_0, z_0)$ as

$$z - z_0 = -(x - x_0)\tan\theta_g. \tag{21}$$

# 4 RESULTS

The simulation of the 6-DOF biped robot has the design parameters [13], footstep variables and terrain parameters [9] as shown in Table 2. The parameters of biped are used to mimic its dynamics using the nonlinear inverted pendulum (NIP) model. The footstep planning with trajectories of the center of mass and contact point of NIP is used to obtain the joint angle trajectories of the 6-DOF biped robot. In inverse kinematics, the center of the hip-link follows the trajectory of the center of mass G, and the relative motion between the center of mass and the hip-link center is assumed to be negligible. Also, the mass of the hip-link is considered significantly large compared to the mass of the legs. The foot-terrain contact forces in the NIP model and the 6-DOF biped robot are modeled using spring-damper of terrain stiffness $k_n$ and $k_t$ in the normal and tangential direction, respectively, and the damping ratio $\zeta$.

**Table 2: Biped robot simulation parameters**

| | |
|---|---|
| Total mass ($m$) | 3.50 kg |
| Mass moment of inertia about $Y_c$ axis ($I_{yy}$) | $1.08 \times 10^{-3}$ kg m$^2$ |
| Mass of hip-link ($m_0$) | 3.45 kg |
| Mass of each leg ($m_l$) | 0.025 kg |
| Thigh length ($L_1$) | 76 mm |
| Shank length ($L_2$) | 76 mm |
| Ankle height from foot ($L_{ah}$) | 32 mm |
| Maximum height of swing leg ankle | 20 mm |
| Foot size | 20 mm × 30 mm |
| Normal stiffness of hard terrain | 49 564.9 N/m |
| Tangential stiffness of hard terrain | 36 793.3 N/m |
| Normal stiffness of deformable terrain | 7105.63 N/m |
| Tangential stiffness of deformable terrain | 5886.93 N/m |
| Damping ratio ($\zeta$) | 0.6 |
| Coefficient of friction ($\mu$) | 0.5 |
| Initial position of center of mass (in m) | (0,0,0.1704) |
| Initial position of hip-link center (in m) | (0,0,0.1726) |
| Initial velocity of hip-link center (in m/s) | (0.4,0,0) |

## 4.1 Footstep planning for equal local energy

The energy curves of the simplified NIP model and foot placement on equal local energy curve for inclined deformable terrain ($\theta_g = 6^o$) are shown in Fig. 2. The trajectory of the center of mass (CoM) and the motion of the NIP are also shown in the figure. The simulation of the dynamics of the robot and the trajectories of the center of the hip-link and the ankles are shown in Fig. 3.

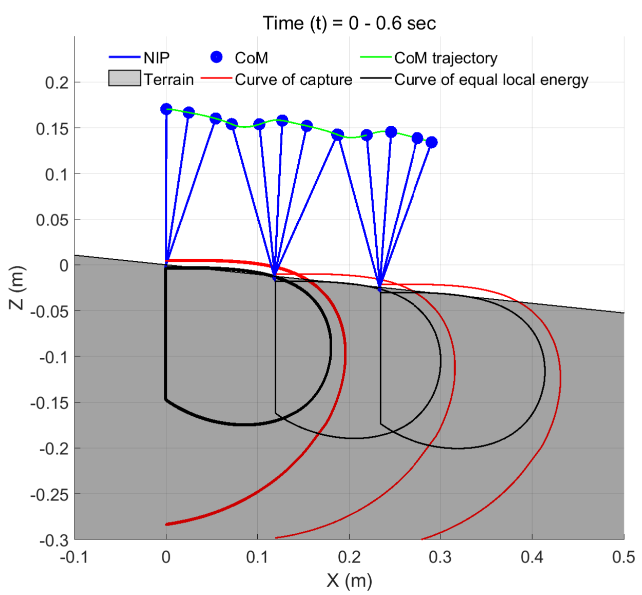


**Figure 2: Foot placement of NIP on equal local energy curve for walking on inclined deformable terrain ($k_n$ = 7105.63 N/m , $k_t$ = 5886.93 N/m and $\zeta$ = 0.6) of slope angle $\theta_g = 6^o$**

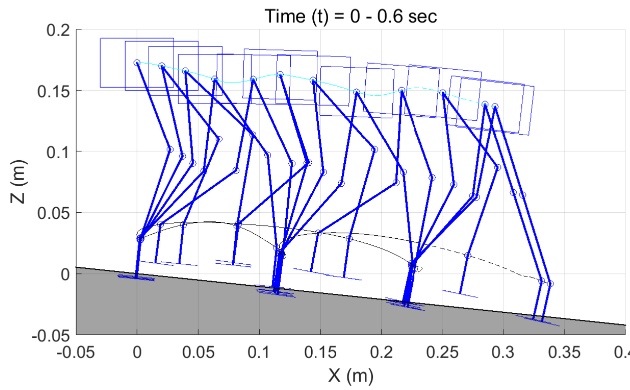


**Figure 3: Biped walking on inclined deformable terrain ($k_n$ = 7105.63 N/m , $k_t$ = 5886.93 N/m and $\zeta$ = 0.6) of slope angle $\theta_g = 6^o$**

The variation of the energy of biped over the period of walking is shown in Fig. 4. It is evident from the figure that the minimum kinetic energy (KE) is equivalent for every step and actuation energy (AE) is negligible for energy-efficient walking. In Fig. 5, the joint torques obtained from inverse dynamics of the biped are plotted.

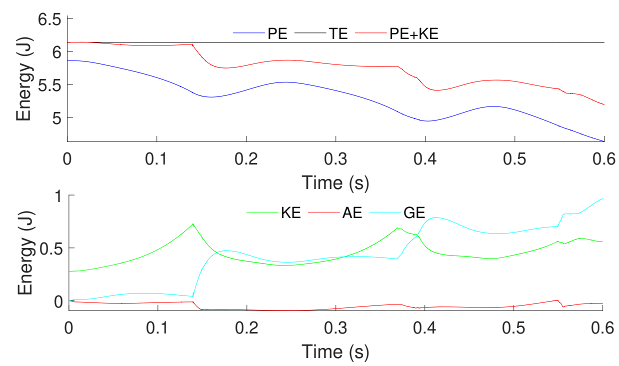


**Figure 4: Variation of potential energy (PE), kinetic energy (KE), actuation energy (AE), ground energy (GE) and total energy (TE) of biped on inclined deformable terrain**

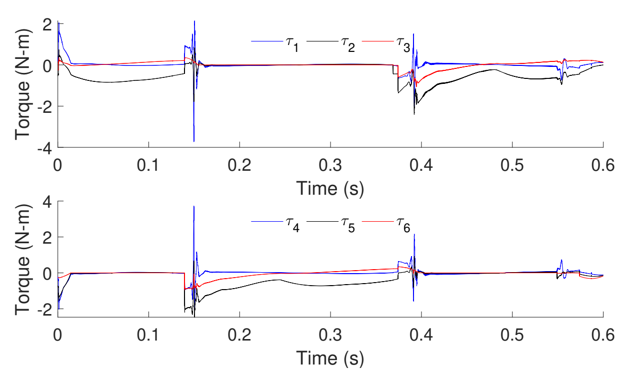


**Figure 5: Joint torques of left ($\tau_{1-3}$) and right ($\tau_{4-6}$) leg**

The biped walking on inclined hard terrain ($\theta_g = 6^o$) is shown in Fig. 6. The variation of kinetic energy (KE), potential energy (PE), actuation energy (AE) and ground energy (GE) are shown in Fig. 7. In Fig. 8, the desired and actual trajectories of the center of mass for walking on inclined deformable and hard terrain are plotted. The comparison of the center of mass trajectory on deformable and hard terrain shows that the increase in deformation of the terrain increases the duration of the double support phase which is not modeled in the simplified dynamics of the NIP model. This duration of the double support phase deviates the actual trajectory of the center of mass from the desired trajectory.

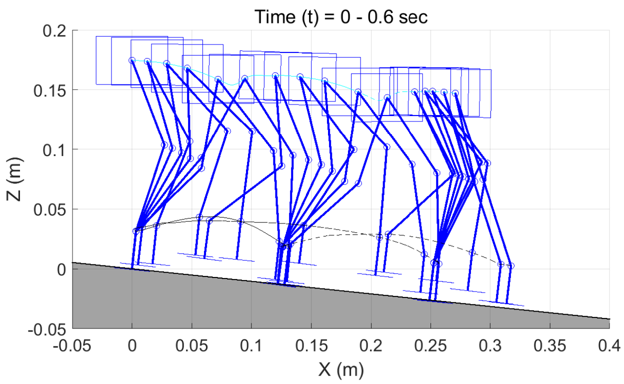


**Figure 6: Biped walking on inclined hard terrain ($k_n$ = 49 564.9 N/m , $k_t$ = 36 793.3 N/m and $\zeta$ = 0.6) of slope angle $\theta_g = 6^o$**

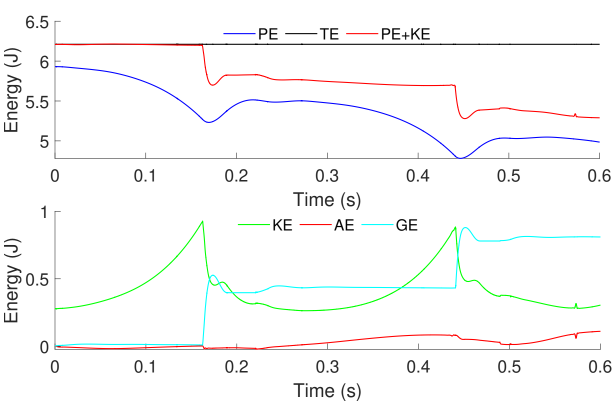


**Figure 7: Energy variation of biped climbing down on inclined hard terrain**

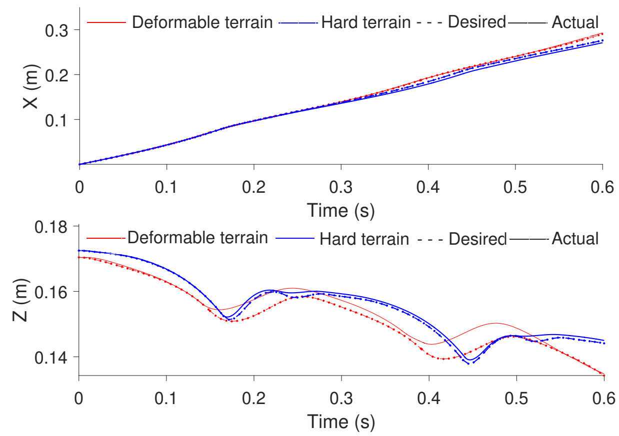


**Figure 8: Center of mass trajectory of biped on inclined deformable and hard terrain**

## 4.2 Capture Point on deformable terrain

The intersection of the capture curve and the terrain is defined as the capture point. The foot placement on the capture point will stop the motion of the biped robot. The joint angle trajectory for foot placement on the capture point is obtained from the motion of the NIP. The biped simulation to stop the motion using capture point on inclined deformable terrain ($\theta_g = 1.8^o$) is shown in Fig. 9. For this motion, the variations in the energy are shown in Fig. 10, in which the kinetic energy reduces to stop the robot's motion.

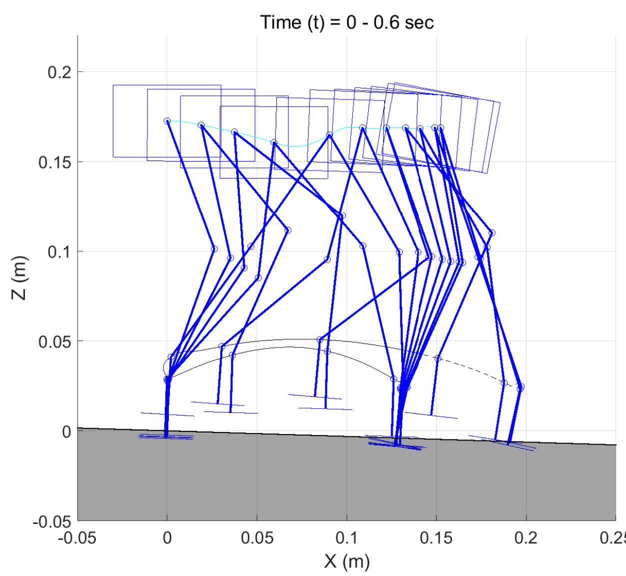


**Figure 9: Biped simulation of foot placement on capture point for walking on inclined deformable terrain ($k_n$ = 7105.63 N/m , $k_t$ = 5886.93 N/m and $\zeta$ = 0.6) of slope angle $\theta_g = 1.8^o$**

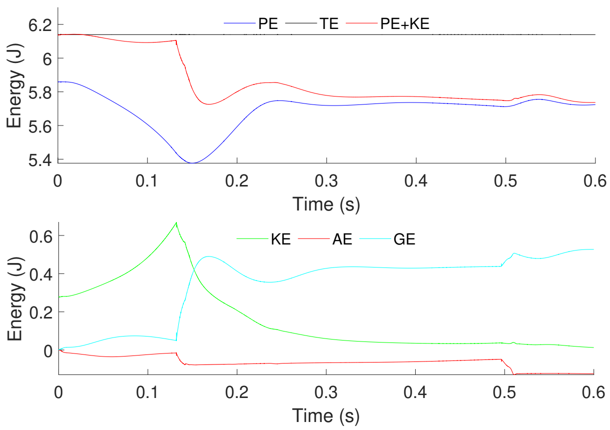


**Figure 10: Energy variation of biped on inclined deformable terrain ($k_n$ = 7105.63 N/m , $k_t$ = 5886.93 N/m and $\zeta$ = 0.6) of slope angle $\theta_g = 1.8^o$**

## 4.3 Stable walking of biped on deformable terrain

The dynamic stability criterion of a biped walking on deformable terrain is defined based on the rotation of the stance leg foot. The foot rotates due to the change of center of pressure while walking on a deformable terrain. Rotation of the foot reduces the effective support area and also destabilizes the robot configuration maintained by joint angles without the center of mass trajectory control. It is to be noted that the simplified dynamics of nonlinear inverted pendulum minimizes the rotation of the foot. The orientations of the foot over the period of walking on inclined hard and deformable terrain are shown in Fig. 11. The figure shows that the foot orientation changes significantly during the leg transition on deformable terrain, which is due to the double support phase not included in the NIP model.

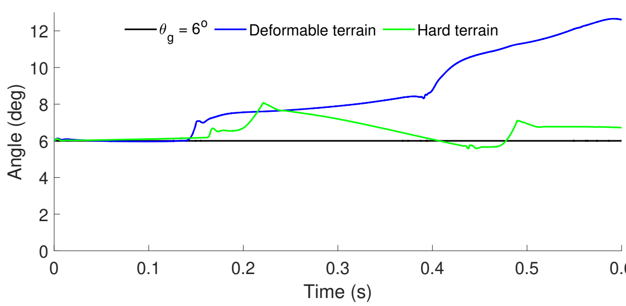


**Figure 11: Orientation of the stance leg foot**

# 5 CONCLUSION

In this work, footstep planning of a NIP is used for generating a gait of a 6-DOF biped robot. In the NIP model, the post-impact angular velocity during the stance leg transition is derived using the conservation of angular momentum. The energy loss is analyzed to obtain the curve of capture and that of equal local energy. The footstep planning on inclined hard and deformable terrain using energy regions is presented. The actual and desired trajectories of the center of mass of the biped on deformable and hard terrain are analyzed to show the effect of terrain deformation. The energy efficiency and dynamic stability of the biped gait on the deformable terrain are also presented. In future work, the footstep planning will be extended for walking on 3D uneven terrain.

# REFERENCES


[1] Joel Chestnutt, Manfred Lau, German Cheung, James Kuffner, Jessica Hodgins, and Takeo Kanade. 2005. Footstep planning for the honda asimo humanoid. In *Proceedings of the 2005 IEEE international conference on robotics and automation*. IEEE, 629–634.

[2] John J Craig. 2009. *Introduction to robotics: mechanics and control, 3/E*. Pearson Education India.

[3] Steven Crews and Matthew Travers. 2020. Energy Management Through Footstep Selection For Bipedal Robots. *IEEE Robotics and Automation Letters* 5, 4 (2020), 5485–5493.

[4] Sunil Gora, Shakti S Gupta, and Ashish Dutta. 2021. Optimal Gait Generation of an 8-DOF Biped Robot on Deformable Terrain using Floating-base Dynamics. In *Advances in Robotics-5th International Conference of The Robotics Society*. 1–6.

[5] Sunil Gora, Shakti S Gupta, and Ashish Dutta. 2023. Energy-Based Footstep Planning of Biped on Uneven Deformable Terrain Using Nonlinear Inverted Pendulum. *Journal of Mechanisms and Robotics* 15, 5 (2023).

[6] Shuuji Kajita, Fumio Kanehiro, Kenji Kaneko, Kazuhito Yokoi, and Hirohisa Hirukawa. 2001. The 3D linear inverted pendulum mode: A simple modeling for a biped walking pattern generation. In *Proceedings 2001 IEEE/RSJ International Conference on Intelligent Robots and Systems. Expanding the Societal Role of Robotics in the the Next Millennium (Cat. No. 01CH37180)*, Vol. 1. IEEE, 239–246.

[7] Scott Kuindersma, Robin Deits, Maurice Fallon, Andrés Valenzuela, Hongkai Dai, Frank Permenter, Twan Koolen, Pat Marion, and Russ Tedrake. 2016. Optimization-based locomotion planning, estimation, and control design for the atlas humanoid robot. *Autonomous robots* 40, 3 (2016), 429–455.

[8] Jitendra Kumar and Ashish Dutta. 2021. Energy optimal motion planning of a 14-DOF biped robot on 3D terrain using a new speed function incorporating biped dynamics and terrain geometry. *Robotica* (2021), 1–29.

[9] T William Lambe and Robert V Whitman. 1991. *Soil mechanics*. Vol. 10. John Wiley & Sons.

[10] Tad McGeer. 1990. Passive dynamic walking. *Int. J. Robotics Res.* 9, 2 (1990), 62–82.

[11] George Mesesan, Johannes Englsberger, Gianluca Garofalo, Christian Ott, and Alin Albu-Schäffer. 2019. Dynamic walking on compliant and uneven terrain using DCM and passivity-based whole-body control. In *2019 IEEE-RAS 19th International Conference on Humanoid Robots (Humanoids)*. IEEE, 25–32.

[12] Jerry Pratt, John Carff, Sergey Drakunov, and Ambarish Goswami. 2006. Capture point: A step toward humanoid push recovery. In *2006 6th IEEE-RAS international conference on humanoid robots*. IEEE, 200–207.

[13] Abhishek Sarkar and Ashish Dutta. 2015. 8-DoF biped robot with compliant-links. *Robotics and Autonomous Systems* 63 (2015), 57–67.

[14] Abhishek Sarkar and Ashish Dutta. 2019. Optimal trajectory generation and design of an 8-dof compliant biped robot for walk on inclined ground. *Journal of Intelligent & Robotic Systems* 94, 3 (2019), 583–602.

[15] Tomoya Sato, Sho Sakaino, Eijiro Ohashi, and Kouhei Ohnishi. 2010. Walking trajectory planning on stairs using virtual slope for biped robots. *IEEE transactions on industrial electronics* 58, 4 (2010), 1385–1396.

[16] Russ Tedrake, Teresa Weirui Zhang, Ming-fai Fong, and H Sebastian Seung. 2004. Actuating a simple 3D passive dynamic walker. In *IEEE International Conference on Robotics and Automation, 2004. Proceedings. ICRA'04. 2004*, Vol. 5. IEEE, 4656–4661.

[17] Miomir Vukobratović and Branislav Borovac. 2004. Zero-moment point—thirty five years of its life. *International journal of humanoid robotics* 1, 01 (2004), 157–173.

[18] Xiaobin Xiong, Aaron D Ames, and Daniel I Goldman. 2017. A stability region criterion for flat-footed bipedal walking on deformable granular terrain. In *2017 IEEE/RSJ International Conference on Intelligent Robots and Systems (IROS)*. IEEE, 4552–4559.

[19] Zhangguo Yu, Xuechao Chen, Qiang Huang, Wen Zhang, Libo Meng, Weimin Zhang, and Junyao Gao. 2015. Gait planning of omnidirectional walk on inclined ground for biped robots. *IEEE Transactions on Systems, Man, and Cybernetics: Systems* 46, 7 (2015), 888–897.